Development and Assessment of Precipitation Products from the Microwave Integrated Retrieval System (MiRS)

Christopher Grassotti[1], Shuyan Liu[2], Junye Chen[1], Quanhua Liu[3]

1. University of Maryland, ESSIC/CICS and NOAA/NESDIS/STAR (christopher.grassotti@noaa.gov) 2. Colorado State University/CIRA and NOAA/NESDIS/STAR 3. NOAA/NESDIS/STAR

1. Background

MiRS (Microwave Integrated Retrieval System) is a One-Dimensional Variational inversion scheme (1DVAR) (Boukabara et al. 2013) that employs the Community Radiative Transfer Model (CRTM) as the forward and adjoint operators. It simultaneously solves for surface (Tskin, emissivity), and atmospheric parameters (temperature, water vapor, non-precipitating cloud and hydrometeor profiles). MiRS is currently being run operationally at NOAA for Suomi-NPP/ATMS, POES N18/N19, Metop-A, Metop-B, DMSP-F17/F18, and Megha-Tropiques/SAPHIR. In August 2016, an updated version (v11.2) was delivered to NOAA operations, extending processing capability to GPM/GMI measurements. The 1DVAR algorithm uses an iterative approach in which a solution is sought that best fits the observed satellite radiances, subject to other constraints. A post-processing step is then performed to determine a number of additional derived parameters, including surface precipitation rate (Iturbide-Sanchez et al. 2011). The precipitation rate determination is sensor-independent in that the same relationships (determined off-line using numerical weather prediction model simulations) between the surface precipitation rate and the vertical hydrometeor profiles are used throughout.

In this poster, we report on assessment and validation of the MiRS precipitation rate product, including comparisons with ground-based measurements such as the Stage IV and MRMS Q3 radar-gauge products, focusing primarily on results from Suomi-NPP/ATMS, and GPM/GMI. Additional discussion will focus on potential avenues for improvement based on results from validation and sensitivity testing.

2. MiRS 1DVar Algorithm

The 1DVAR algorithm uses an iterative approach in which a solution is sought which "best fits" the observed satellite radiances, subject to other constraints. To reach the iterative solution, the algorithm seeks to minimize the cost function

$$J(X)=\left[\frac{1}{2}(X-X_0)^T\times B^{-1}\times(X-X_0)\right]+\left[\frac{1}{2}(Y^m-Y(X))^T\times E^{-1}\times(Y^m-Y(X))\right]$$

where X in the 1st term on the right is the retrieved state vector, and the term itself represents the penalty for departing from the background X_0, weighted by the error covariance matrix B. The 2nd term represents the penalty for the simulated radiances Y departing from the observed radiances Y^m, weighted by instrument and modeling errors E. This leads to the iterative solution

$$\Delta X_{n+1}=\left\{BK_n^T\left(K_nBK_n^T+E\right)^{-1}\right\}\left[\left(Y^m-Y(X_n)\right)+K_n\Delta X_n\right]$$

where ΔX is the updated state vector at iteration n+1, and K is the matrix of Jacobians which contain the sensitivity of the radiances to changes in X (parameters to retrieve). This is then followed by the post-processing step which uses as inputs the elements of the state vector X. Figure 1 summarizes the MiRS processing components.

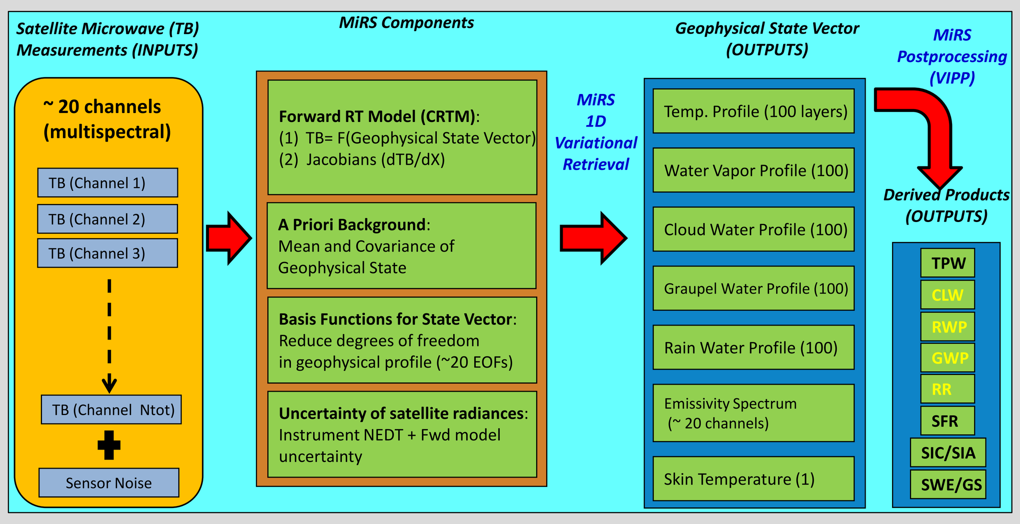

Figure 1. MiRS core retrieval and post-processing (VIPP) components. Core products are retrieved simultaneously as part of the state vector. VIPP products are derived through vertical integration (hydrometeors), catalogs (SIC, SWE), or fast regressions (Rain Rate). Hydrometeor retrieval products are indicated in yellow: Rain Rate, Graupel Water Path, Rain Water Path and Cloud Liquid Water.

Post-processing to determine a surface precipitation rate is done by first vertically integrating each of the cloud (small droplets of 30 microns), as well as the precipitation-related profiles of rain water and graupel water (500 microns) to obtain CLW, RWP, and GWP, respectively. The rain rate is then computed from the following equations:

$$RR(CLW,RWP,GWP)=RR_{CLW}+3.879*(RWP+GWP)^{1.103}$$

$$\text{where}\quad RR_{CLW}=2.339*(CLW)^{1.156}$$

The relationship between RR and CLW, RWP, and GWP is based on off-line simulations of the MM5 mesoscale model for a number of cases. The same equation is applied for all operational satellites, and over all surface types, with the exception that over land the CLW-based term is set to zero, since it had been previously determined that CLW microwave signal over land was low relative to variations in background surface emissivity. However, recent testing indicates that use of CLW may improve light rain detection and estimation over land. (see Section TBD)

3. CRTM Hydrometeor Jacobians

All versions of MiRS starting with v11.0 utilize Version 2.1.1 of CRTM. The key element of CRTM that allows for the rapid retrieval of not only the temperature and water vapor profile, but also the liquid and frozen hydrometeor profiles is the simultaneous computation of both forward simulated radiances, and their corresponding Jacobians (sensitivity of radiances with respect to retrieval state vector). The scattering calculation in this version of CRTM assumes spherical particles (Mie approximation). Upcoming versions of CRTM will incorporate non-spherical particles.

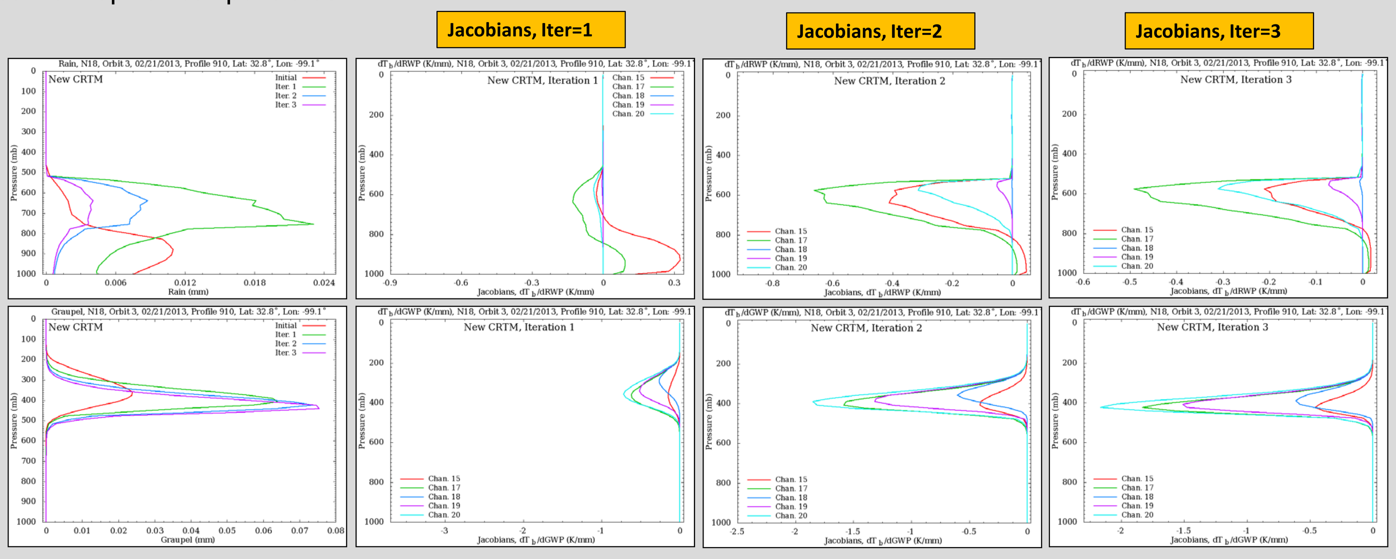

Evolution of retrieved rain and graupel water and associated Jacobians show (1) non-linear behavior in that Jacobian profile changes with hydrometeor amount, and (2) final retrieved profile can have different shape than a priori background/first guess.

Figure 2. Example of rain water (top) and graupel water (bottom) retrieval evolution for a single profile based on NOAA-18 AMSU-MHS measurements. Left panels show rain and graupel water profile retrieval as function of iteration (3 iterations total). The remaining panels show the CRTM Jacobians with respect to rain and graupel at channels 15, 17, 18, 19, 20 (89, 157, 183±1, 183±3, and 190 GHz), for each iteration. In this case, the retrieval converged in 3 iterations. Rain and graupel particle effective radii were assumed to be 500 microns.

4. MiRS Global Precipitation from ATMS and GMI

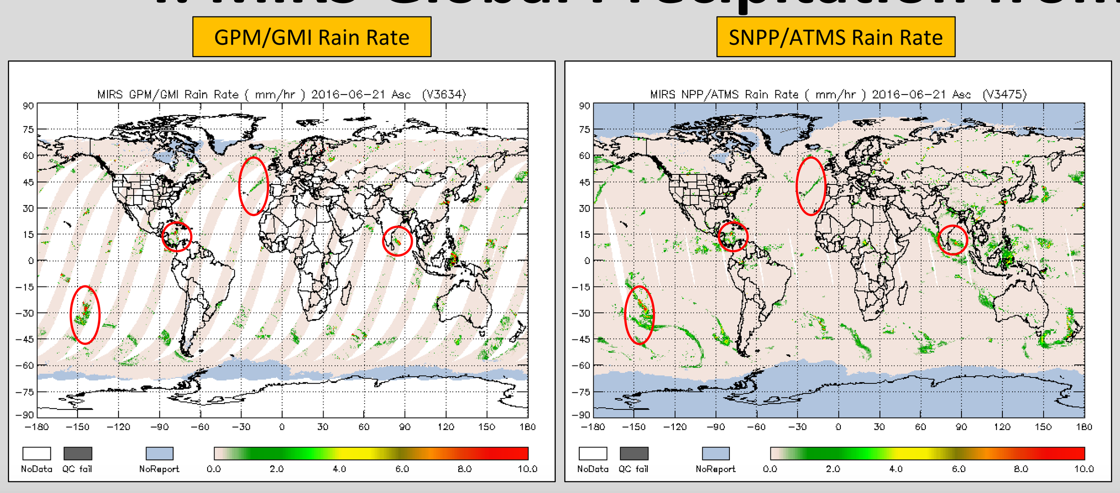

Figure 3. Comparison of global rain rate maps on 21 June 2016 from MiRS when applied to GPM/GMI (left) and SNPP/ATMS measurements (right). Examples of weather systems detected by both satellites are circled.

5. SNPP/ATMS Baseline Comparisons with Stage IV and GPROF

Product	Units	Bias (Accuracy)		StDv (Precision)		Npts
		MiRS	Req	MiRS	Req	
Rain Rate (land, Stage IV)	mm/h	0.01	0.05	0.8	1.5	8.7E+06
Rain Rate (ocean, Stage IV)	mm/h	0.08	0.10	1.0	1.0	1.8E+06
Rain Rate (land, GPROF)	mm/h	-0.01	0.05	0.4	1.5	8.1E+04
Rain Rate (ocean, GPROF)	mm/h	-0.01	0.10	0.8	1.0	1.8E+05

Table 1. Collocation statistics for MiRS SNPP/ATMS rain rate with Stage IV radar-gauge (CONUS) and GPROF-GMI (global) estimates for the period August 2015-March 2016. For each comparison, the JPSS performance requirement is also shown.

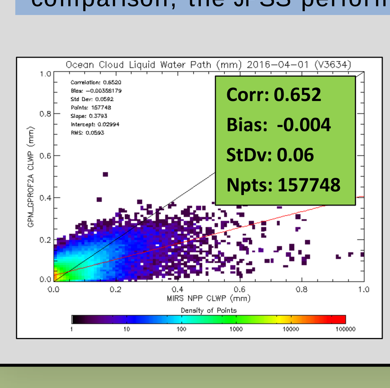

CLW: MiRS and GPROF Ocean

Figure 4. Scatterplot of MiRS SNPP/ATMS CLW (mm) retrievals over ocean vs. GPROF-GMI for the period August 2015-March 2016.

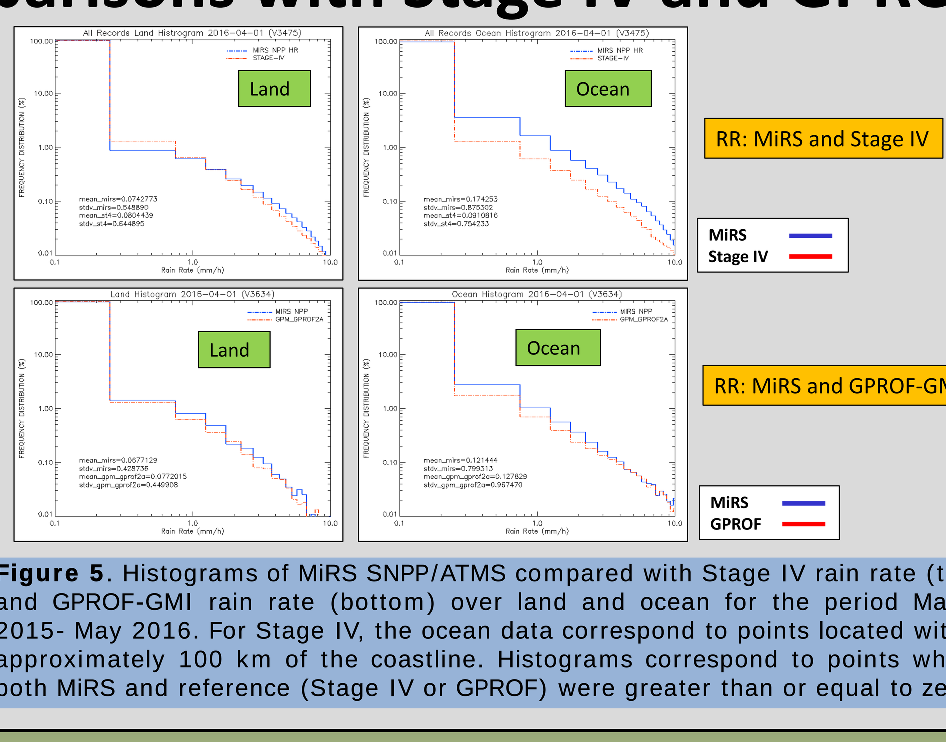

Figure 5. Histograms of MiRS SNPP/ATMS compared with Stage IV rain rate (top) and GPROF-GMI rain rate (bottom) over land and ocean for the period March 2015- May 2016. For Stage IV, the ocean data correspond to points located within approximately 100 km of the coastline. Histograms correspond to points where both MiRS and reference (Stage IV or GPROF) were greater than or equal to zero.

6. Baseline Performance of MIRS GPM/GMI

The primary change in v11.2 is the extension of MiRS to GPM/GMI measurements. Validation activities are continuing with the goal to determine performance in different seasons.

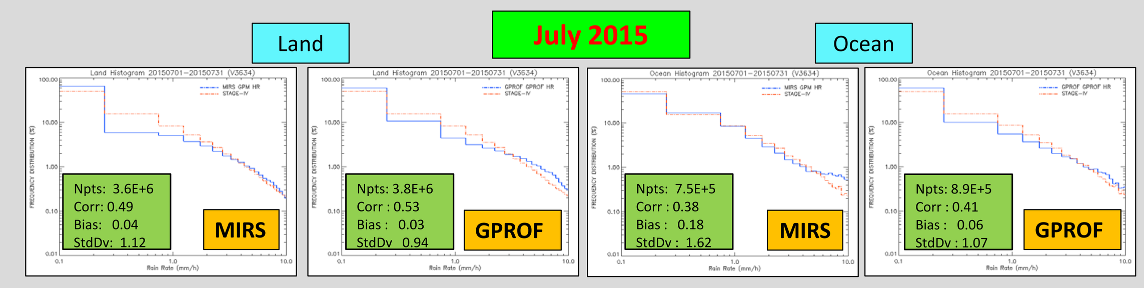

Figure 6. Performance of MiRS and GPROF (v04) GMI relative to Stage IV during July 2015. Histograms are for points when either estimate was greater than 0.

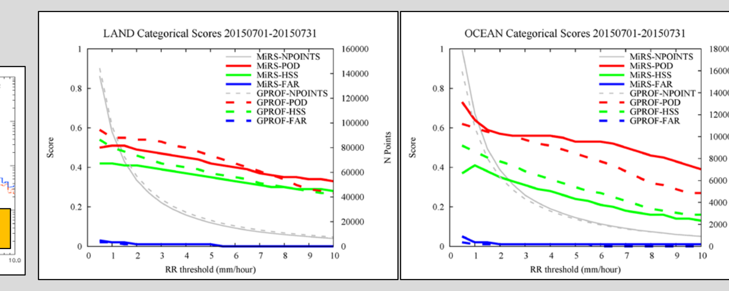

Figure 7. Categorical scores of MiRS and GPROF (v04) GMI relative to Stage IV during July 2015.

MiRS appears to have lower detection of rainfall over land than GPROF, but generally higher over ocean. Slightly higher false alarms reduce the MiRS Heidke Scores. The issue of light rain detection over land is treated in the following section below.

7. Evaluation of CLW/Light Rain Detection over Land

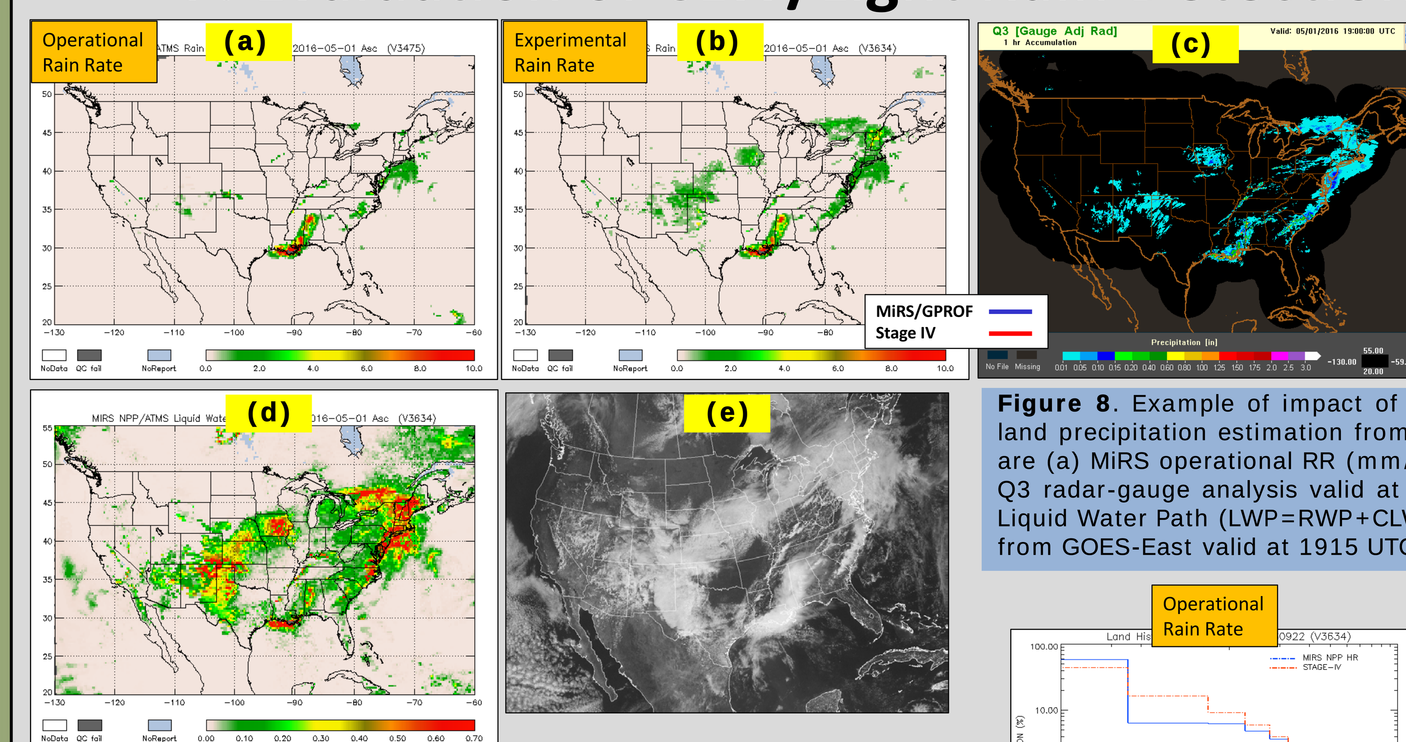

The incorporation of CLW (non-scattering cloud droplets of 30 micron effective radius) into the SNPP/ATMS rain rate estimate clearly improves the detection and estimation of light rainfall over land in this case. The signal of light rain in the CLW retrievals is generally large enough to overcome the increased uncertainty (partly due to higher and more variable land surface emissivity) in the CLW estimates over land.

Figure 8. Example of impact of using retrieved CLW over land in the land precipitation estimation from SNPP/ATMS on 01 May 2016. Shown are (a) MiRS operational RR (mm/h), (b) MiRS RR using CLW, (c) MRMS Q3 radar-gauge analysis valid at 1900 UTC (units in inches), (d) MiRS Liquid Water Path (LWP=RWP+CLW, mm), and (e) visible satellite image from GOES-East valid at 1915 UTC.

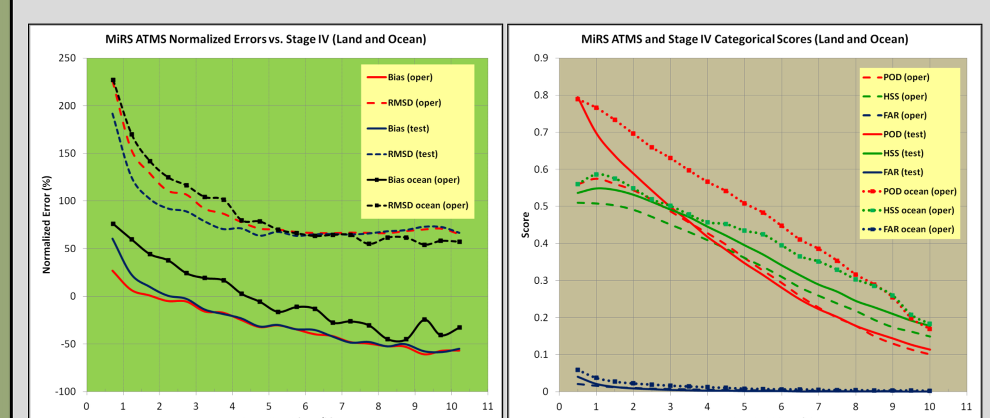

Figure 9. Normalized errors relative to Stage IV in retrieved rain rate (left) and categorical scores (right) for MiRS ATMS retrievals during the period 1-22 Sept 2016 over the CONUS and coastal ocean.

Incorporation of CLW has (1) reduced the normalized bias for land rain rates below 3 mm/h, and the RMSD for rates below 5 mm/h, (2) improved the POD and Heidke Score for most rain rate thresholds.

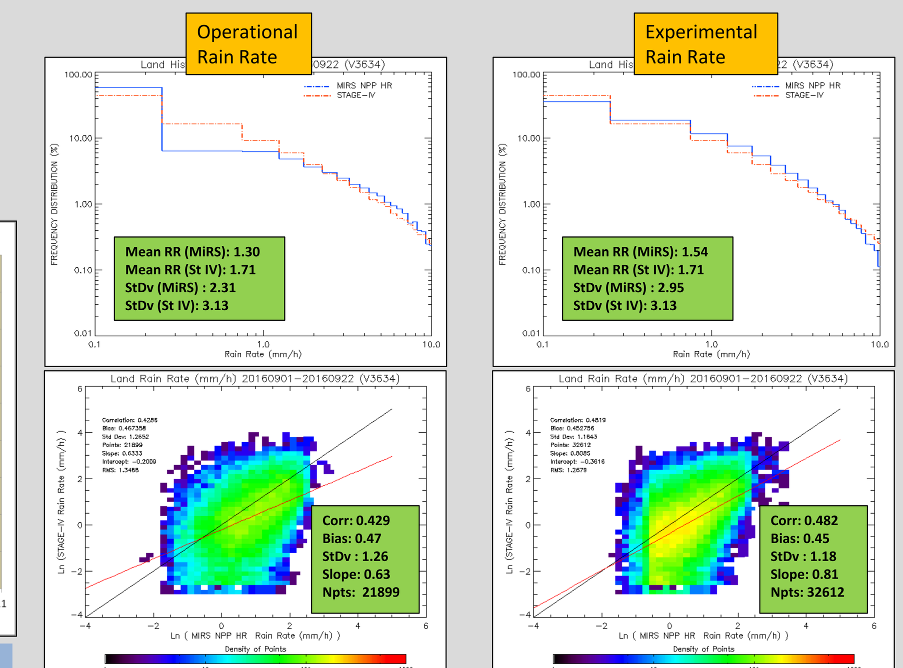

Figure 10. Histograms and scatterplots of MIRS ATMS vs. Stage IV operational and experimental rain rate over land during 1-22 Sept 2016. Note improved frequency distribution and agreement with Stage IV in experimental rain rate, and the large increase in points with RR > 0. Histograms are for all points with Stage IV greater than 0.

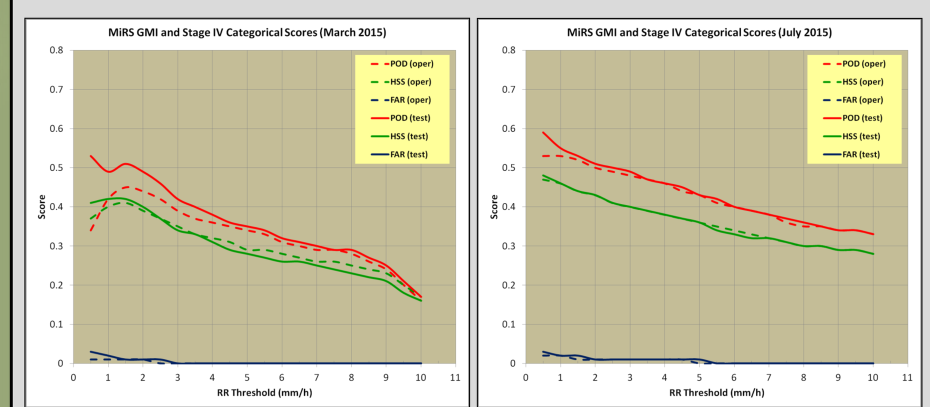

Figure 11. Categorical scores for MIRS GMI operational and test rain rates over land for March and July 2015.

Improvement in light rain detection when CLW is used is greater in March, which typically has a greater percentage of stratiform rain events.

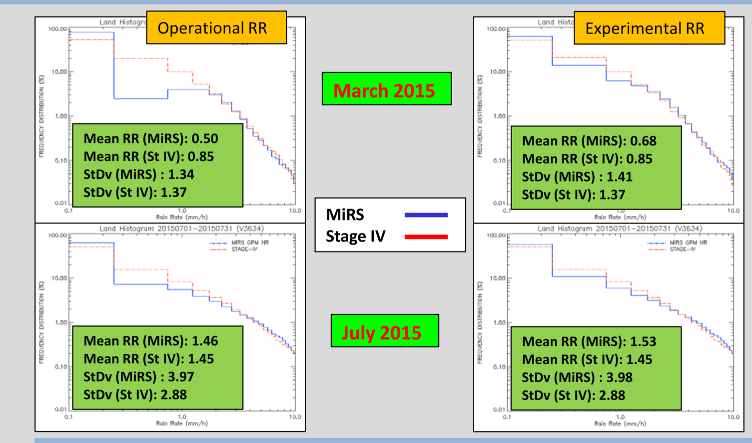

Figure 12. Histograms for MIRS GMI operational and experimental rain rates over land for March and July 2015.

8. Tropical Cyclone Warm Core Structure

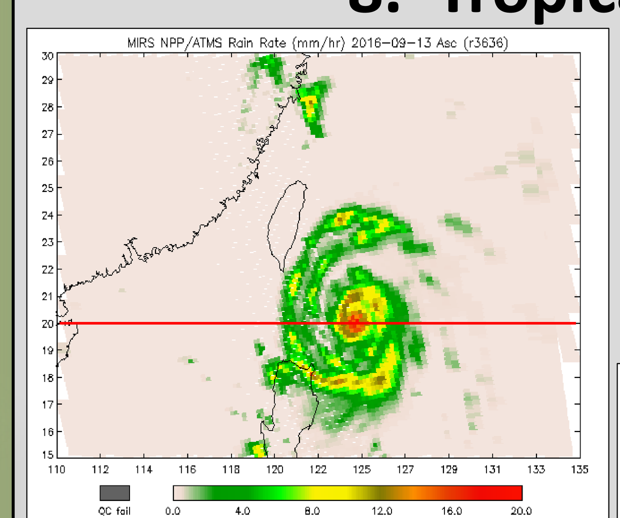

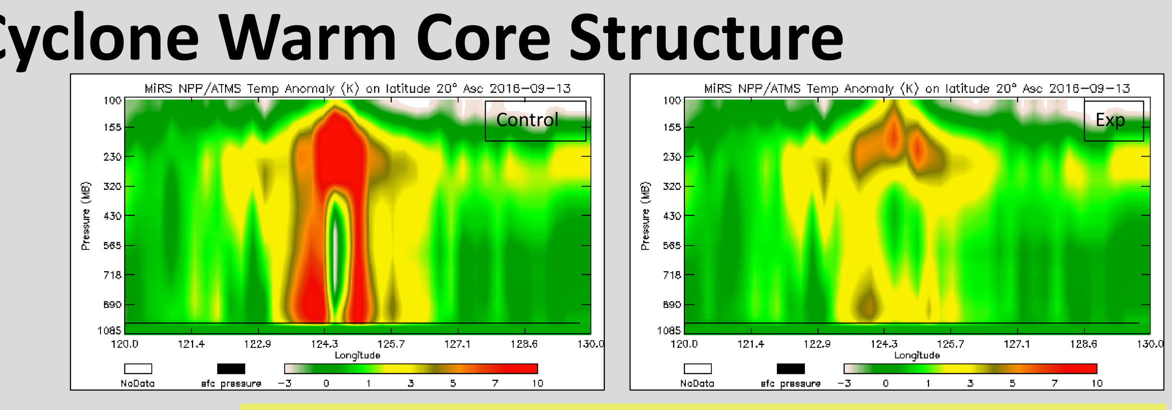

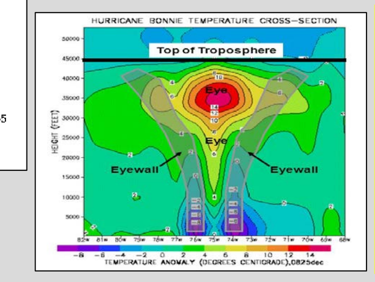

*In operational retrieval (**Control,** top center) the temperature profile was retrieved normally, accounting for climatological covariances between temperature and other parameters such as water vapor and hydrometeors. The unrealistic low level warm anomaly is partly an artifact of the rain signal in the measured radiances. In experimental retrieval (**Exp,** top right) the temperature was assumed uncorrelated with all other retrieved parameters. This decorrelation results in a temperature anomaly structure closer to the expected one (see example at left), with the warmest anomalies concentrated near the tropopause, and decreasing at lower levels. The improvement is consistent with the fact that the atmospheric structure of tropical cyclones is fundamentally different than that for global average conditions.*

Figure 13. MiRS retrievals of rain rate and temperature structure for Typhoon Meranti on 13 September 2016. Top Left: MiRS rain rate (mm/h) with location of cross-section indicated. Top center: Operational (Control) retrieval of temperature anomaly cross-section. Top right: Experimental (Exp) version of temperature anomaly cross-section. Bottom center: Typical temperature anomaly cross-section.

9. Summary

A new version of the NOAA MiRS algorithm (V11.2) has recently been released and will be transitioned to operations at NOAA. Work is ongoing to assess, validate and improve the precipitation products from MiRS.

- MiRS has now been extended to routinely process data from GPM/GMI making a total of 9 satellites processed by the MiRS algorithm operationally by NOAA.
- Rainfall retrievals over ocean show satisfactory performance in terms of error statistics (bias, standard deviation, correlation), as well as contingency-based metrics.
- Detection and estimation of light precipitation (< 3 mm/h) over land has been improved by the incorporation of non-scattering cloud water in the rainfall rate relationships.
- Experiments are ongoing to improve the retrieved temperature structure in and around tropical cyclones, for example, by modifying the assumed intercorrelations between temperature, water vapor, and hydrometeors, to better match tropical cyclone climatologies.

Future Work:
- Leverage planned improvements to CRTM, e.g. non-spherical particle scattering.
- Incorporation of hydrometeor effective radius as variable in state vector (currently fixed at 500 microns).
- Development of a priori constraints to improve T and WV retrievals in rainy conditions.
- Extension of MiRS operational capability to to upcoming JPSS-1/ATMS mission data by 2017.

Access to MiRS data and software: (1) MiRS website at mirs.nesdis.noaa.gov, (2) NOAA CLASS archive at www.class.noaa.gov, (3) Direct Broadcast Package: CSPP_MIRS_2.0 at cimss.ssec.wisc.edu/cspp

10. Acknowledgements

Work supported in part by CICS Award NA14NES4320003 (CICS Cooperative Agreement 2014-2019).

11. References

Boukabara et al., 2013: A physical approach for a simultaneous retrieval of sounding, surface, hydrometeor, and cryospheric parameters from SNPP/ATMS, J. Geophys. Res. Atmos., 118, 12,600–12,619, doi:10.1002/2013JD020448.

Iturbide-Sanchez et al., 2011: Assessment of a Variational Inversion System for Rainfall Rate Over Land and Water Surfaces. IEEE Trans. Geosci. Remote Sens., 49 (9), 3311-3333, doi: 10.1109/TGRS.2011.2219375